

## 基于 Sagnac 干涉仪的光纤耦合器耦合相移检测技术

王瑞琴, 杨远洪\*, 李慧

北京航空航天大学仪器科学与光电工程学院, 北京 100191

**摘要** 提出了一种基于混合 Sagnac 干涉仪的光纤耦合器耦合相移检测技术, 其中混合 Sagnac 干涉仪由待测单模光纤耦合器和保偏光纤组成。基于混合 Sagnac 干涉仪互易端口和非互易端口输出干涉光谱的谷值波长特征, 推导出单模光纤耦合器耦合相移检测方程并进行了测试误差分析。搭建了实验系统, 实现了固定分光比  $3 \times 3$  单模耦合器以及不同分光比  $2 \times 2$  单模耦合器耦合相移的高精度检测, 并首次实现了不同温度条件下  $2 \times 2$  单模耦合器的耦合相移变化特性测量, 实验结果与理论估计一致。理论分析和实验研究结果表明, 所提检测方法实施方便、检测精度高, 适应性强, 为光纤耦合器耦合相移的定量精确测试和分析提供了有效手段。

**关键词** 光纤光学; 单模光纤耦合器; 耦合相移; Sagnac 干涉仪

中图分类号 TN253

文献标志码 A

DOI: 10.3788/CJL202249.0906001

### 1 引言

光纤耦合器是光纤通信和传感系统中的基础器件, 主要性能指标有附加损耗、分光比、工作波长<sup>[1]</sup>等, 是组成马赫-曾德尔干涉仪、迈克耳孙干涉仪和光纤陀螺等仪器<sup>[2-6]</sup>的核心器件。除上述指标外, 耦合器各端口之间的相位关系, 即耦合相移, 也会对传感系统的性能产生明显影响<sup>[7-9]</sup>。精确测定光纤耦合器的耦合相移及其变化特性对研制高性能光纤耦合器、提高光纤干涉仪及其应用系统的性能具有重要价值。1982 年, Priest<sup>[10]</sup>首次利用散射矩阵对无损耗情况下耦合器的相移特性进行了理论分析, 这一分析方法直观简便, 分析结果与实验现象有较高的吻合度, 是耦合器理论分析的主流方法。随后, 研究者引入了附加损耗<sup>[11]</sup>、对称性<sup>[12]</sup>等因素, 完善了耦合器相移的分析理论。但理论分析过程均存在较多的理想假设, 导致计算结果与真实相移仍存在一定差距, 且耦合器的相移受温度、光波长等外界因素的影响, 理论分析只能根据其本征特性确定相移的大致范围, 确切的耦合相移值必须通过实验检测来确定。

1988 年, Gottwald 等<sup>[13]</sup>基于光纤马赫-曾德尔

干涉仪, 采用光源调制技术, 通过测量各端口的输出光功率来计算耦合相移, 首次实现了  $3 \times 3$  单模光纤耦合器的耦合相移检测。Schliep 等<sup>[14-15]</sup>同样基于马赫-曾德尔干涉仪, 采用相位调制技术, 实现了  $2 \times 2$  和  $3 \times 3$  单模光纤耦合器的耦合相移检测。该技术利用压电陶瓷对参考臂长度进行调制, 相对光源调制更加简便, 但仍通过强度解调来得到相移值, 检测精度受到光电转换、光路损耗、分光耦合器性能、调制信号等因素的影响, 存在较大误差。随着信号解调技术的发展, 研究者在上述检测结构的基础上, 提出了对输出信号进行 Bessel 展开<sup>[16]</sup>或傅里叶变换<sup>[17]</sup>的解调算法, 以去除输出功率中光源波动、光路损耗以及光电转换等无关因素的影响, 提高了耦合器相移的检测精度, 报道的最高检测精度为  $0.229^\circ$ <sup>[17]</sup>。

本文提出了一种基于混合 Sagnac 干涉仪的光纤耦合器耦合相移检测技术, 其中混合 Sagnac 干涉仪由待测单模光纤耦合器和保偏光纤组成。通过测量耦合器互易端口和非互易端口的输出干涉光谱, 基于这两个光谱的谷值波长特征, 推导出单模光纤耦合器的相移检测方程并进行了测试误差分析。该检测方法通过提取光谱的特征波长来实现耦合相移

收稿日期: 2021-08-09; 修回日期: 2021-09-28; 录用日期: 2021-10-18

基金项目: 国家自然科学基金(61227902, U1637106)、国家重点研发计划(2018YFC1503703)、创新团队发展计划(IRT 1203)

通信作者: \*yhyang@buaa.edu.cn

的检测,相对强度解调具有更好的抗干扰性及检测精度,且能消除互易型相位干扰带来的误差。搭建了实验系统,实现了常用的固定分光比  $3 \times 3$  单模光纤耦合器以及不同分光比的  $2 \times 2$  单模光纤耦合器耦合相移的检测。在此基础上,研究了不同温度条件下  $2 \times 2$  单模耦合器的耦合相移变化特性。所提出的检测技术具有实施方便、检测精度高、适应性强的优势,可用于各类单模光纤耦合器耦合相移的检测。

## 2 理论分析及检测原理

### 2.1 耦合器相移理论

当光纤耦合器用于干涉仪光路时,各端口之

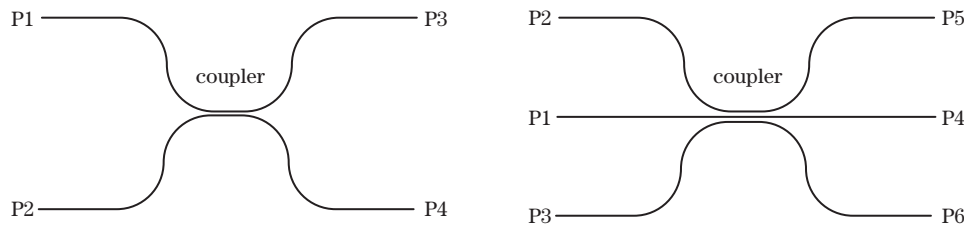


图 1 光纤耦合器结构示意图。(a)  $2 \times 2$  耦合器;(b)  $3 \times 3$  耦合器

Fig. 1 Structural diagram of optical fiber coupler. (a)  $2 \times 2$  coupler; (b)  $3 \times 3$  coupler

张清华<sup>[18]</sup>基于光纤耦合器散射矩阵分析法,对耦合器相移特性进行了较全面的研究,用散射矩阵描述了光纤耦合器传输的光束在耦合区域发生能量交换的过程:

$$\mathbf{S} = [s_{ij}]_{2n \times 2n}, \quad (2)$$

式中: $\mathbf{S}$  为耦合器的散射矩阵; $n$  为耦合器端口数; $i, j$  为耦合器的端口标号; $s_{ij} = |s_{ij}| e^{j\varphi_{ij}}$ , 其中  $|s_{ij}|^2 =$

间的相位关系即耦合相移会对传感系统的性能产生明显影响,是必须明确和测定的重要参数。图 1 所示为  $2 \times 2$  和  $3 \times 3$  光纤耦合器示意图。光从某一端口输入、从同一光纤输出的光路为直通臂,如  $2 \times 2$  耦合器的端口  $P1 \rightarrow$  端口  $P3$ ; 耦合到另一光纤输出的光路为耦合臂,如  $2 \times 2$  耦合器的端口  $P1 \rightarrow$  端口  $P4$ 。一般情况下,耦合相移是指直通臂与耦合臂对应输出端口之间的相位差  $\Delta\varphi$ , 可表示为

$$\Delta\varphi = \varphi_{13} - \varphi_{14} = \varphi_{24} - \varphi_{23}, \quad (1)$$

式中: $\varphi_{13}$ 、 $\varphi_{24}$  为直通臂相位; $\varphi_{14}$ 、 $\varphi_{23}$  为耦合臂相位。

$W_j/W_i$  为耦合效率,  $W_i$  为端口  $i$  的输入功率; $W_j$  为端口  $j$  的输出功率, $\varphi_{ij}$  为光束从耦合器端口  $i$  传输到端口  $j$  所产生的相移。根据 Hermite 矩阵的限制条件即各阶主子式均为正,可以得到耦合相移值理论范围的估算模型<sup>[18]</sup>。设光从  $P1$  输入,经耦合器后从  $P3$  和  $P4$  输出,解得  $2 \times 2$  光纤耦合器耦合相移的理论范围为

$$-\frac{W}{2 |s_{13}| \cdot |s_{14}|} \leq \cos(\Delta\varphi) \leq \frac{W}{2 |s_{13}| \cdot |s_{14}|}, \quad (3)$$

$$W = 1 - |s_{13}|^2 - |s_{14}|^2, \quad (4)$$

式中: $W$  为耦合器的附加损耗。由式(3)可知,对于  $2 \times 2$  耦合器,当不考虑附加损耗 ( $W = 0$ ) 时,  $\cos(\Delta\varphi) = 0$ ,  $\Delta\varphi = \pi/2$ , 即耦合相移恒为  $90^\circ$ , 与分光比无关;但当损耗不为 0 时,实际耦合相移偏离理想值。

在  $3 \times 3$  耦合器中,设光从  $P1$  输入,从  $P4 \sim P6$  输出,则耦合相移的理论范围<sup>[18]</sup>为

$$\frac{-W - |s_{15}|^2}{2 |s_{14}| \cdot |s_{15}|} \leq \cos(\Delta\varphi) \leq \frac{W/2 - |s_{15}|^2}{2 |s_{14}| \cdot |s_{15}|}. \quad (5)$$

由式(5)可知,当不考虑附加损耗且分光比均为  $1/3$  时,  $\cos(\Delta\varphi) = -1/2$ ,  $\Delta\varphi = \pm 2\pi/3$ , 即三个输出端

之间的相位差应互为  $120^\circ$ 。

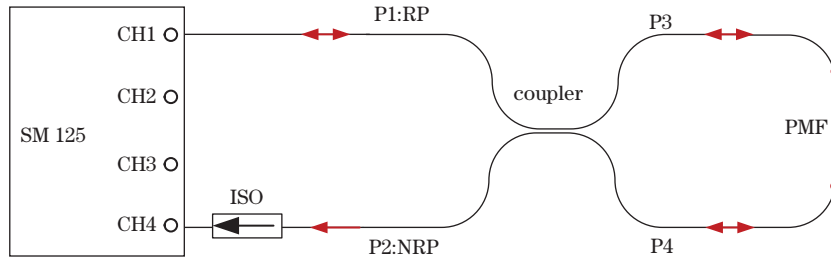
由理论分析结果可得,单模光纤耦合器的耦合相移及其变化范围主要由分光路数和附加损耗决定,引起上述因子发生变化的外界因素(如温度等)也会导致耦合器相移的波动。理论分析只能根据其固有参数估算相移的变化范围,无法得到实际的耦合相移值,耦合器的实际耦合相移及其变化特性需要通过实际测试获得。

### 2.2 耦合相移检测原理

以  $2 \times 2$  单模耦合器为待测件,基于混合 Sagnac 干涉仪的单模耦合器耦合相移检测原理如图 2 所示,混合 Sagnac 干涉仪由待测单模光纤耦合器和保偏光纤(PMF)组成,光源从  $P1$  输入,经耦合

器后分为两束光由 P3、P4 输出,分别沿 Sagnac 环顺时针和逆时针方向传输,然后在光纤耦合器处相遇并发生干涉,干涉信号由 P1、P2 端口输出。其中,端口 P1 为光源输入和信号输出的公共端口,通常被称为互易端口(RP)<sup>[19]</sup>,在这个端口发生干涉的两束光在经过耦合器时,均会经历一次直通和一次耦合,两束光在耦合器光路部分是互易的,该端口输出的干涉信号为环中保偏光纤两偏振模式的干涉光谱,不受耦合器耦合相移的影响,因此在测试中将

这个端口输出的干涉谱作为基准;另一端 P2 仅作为信号输出端口,称为非互易端口(NRP),在这个端口发生干涉的两束光在经过耦合器时,一束光将经历两次直通、另一束光将经历两次耦合,会产生 2 倍耦合相移的附加相位差,这个端口的输出干涉光谱为互易端口 P1 输出光谱的平移结果,平移量为 2 倍耦合相移对应的波长变化量。因此,通过同步测量两端口的光谱,可以计算得到待测耦合器的耦合相移值。



ISO: isolator; RP: reciprocity port; NRP: non-reciprocity port; PMF: polarization maintaining fiber

图 2 基于混合 Sagnac 干涉仪的单模光纤耦合器耦合相移检测原理图

Fig. 2 Principle diagram of coupling phase shift detection of single-mode optical fiber coupler based on hybrid Sagnac interferometer

为了实现两个端口光谱的同步高分辨率测量,采用了美国 Micron Optics 公司生产的光纤光谱解调仪 SM125,它是一种基于可调谐窄线宽激光器可实现宽光谱范围扫描与同步探测的无源器件(光纤光栅、光滤波器等)反射光谱测量仪器,能同步测量各通道反射光谱并给出光谱对应的峰值或谷值波长<sup>[20]</sup>,波长分辨率和精度均能达到 1 pm。如图 2 所示,将 SM125 的一个通道(CH1)与干涉仪端口 P1 连接,实现互易端口光谱测量;将 SM125 的另一通道(CH4)通过光纤隔离器(ISO)与干涉仪端口 P2 连接,实现非互易端口光谱测量,ISO 用于隔离 SM125 的输出光,使 P2 输出干涉光单向传输到解调仪,消除 CH4 输出光的干扰。根据上述分析及干涉公式<sup>[21-22]</sup>,可得互易端口和非互易端口输出干涉信号的表达式分别为

$$P_{RP}(\lambda) = P_0 + P_0 \cos\left(\frac{2\pi\Delta nL}{\lambda}\right), \quad (6)$$

$$P_{NRP}(\lambda) = P_0 + P_0 \cos\left(\frac{2\pi\Delta nL}{\lambda} + 2\Delta\varphi\right), \quad (7)$$

式中: $P_{RP}(\lambda)$ 、 $P_{NRP}(\lambda)$ 分别为互易端和非互易端的输出光谱功率; $P_0$ 为强度系数; $\Delta\varphi$ 为待测耦合器的耦合相移; $\Delta n$ 为保偏光纤快慢轴的折射率差; $L$ 为保偏光纤的长度; $\lambda$ 为光波长。

如图 3 所示,以互易端输出光谱为基准,由于干涉光谱的周期性可知,RP 曲线上相邻谷值波长( $\lambda_1$ 、

$\lambda_3$ )对应的相位差为  $2\pi$ ,即

$$\frac{2\pi\Delta nL}{\lambda_1} - \frac{2\pi\Delta nL}{\lambda_3} = 2\pi. \quad (8)$$

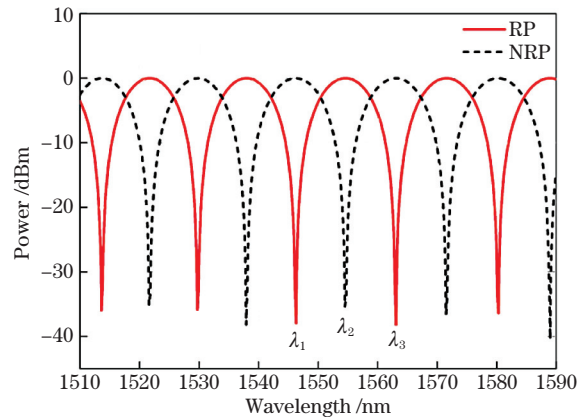


图 3  $2 \times 2$  耦合器混合 Sagnac 光纤干涉仪的理论输出光谱  
Fig. 3 Theoretical output spectra of hybrid Sagnac interferometer with  $2 \times 2$  coupler

由式(6)、(7)可得,位于上述 RP 曲线谷值波长区间内的 NRP 曲线的谷值波长( $\lambda_2$ )和  $\lambda_1$  具有如下关系:

$$2\Delta\varphi + \frac{2\pi\Delta nL}{\lambda_2} = \frac{2\pi\Delta nL}{\lambda_1}. \quad (9)$$

式(8)、(9)联立可得到耦合相移  $\Delta\varphi$  的计算公式为

$$\Delta\varphi = \pi \cdot \frac{\lambda_3}{\lambda_2} \cdot \frac{\lambda_2 - \lambda_1}{\lambda_3 - \lambda_1}. \quad (10)$$

由此,通过测量混合 Sagnac 干涉仪互易端和非互易端的干涉光谱,提取其对应的相邻特征谷值波长( $\lambda_1$ 、 $\lambda_2$ 、 $\lambda_3$ ),根据式(10)即可计算得到待测单模

耦合器的耦合相移。由式(10)可知,耦合相移的检测精度主要由谷值波长的测量精度决定。根据误差分析理论<sup>[23]</sup>,可得耦合相移的极限误差为

$$\delta_{\max}(\Delta\varphi) = e_{\lambda} \sqrt{\left(\frac{\partial\Delta\varphi}{\partial\lambda_1}\right)^2 + \left(\frac{\partial\Delta\varphi}{\partial\lambda_2}\right)^2 + \left(\frac{\partial\Delta\varphi}{\partial\lambda_3}\right)^2} = \frac{\pi \cdot e_{\lambda}}{[\lambda_2(\lambda_3 - \lambda_1)]^2} \cdot \sqrt{(\lambda_2^2\lambda_3 - \lambda_3^2\lambda_2)^2 + (\lambda_1^2\lambda_3 - \lambda_3^2\lambda_1)^2 + (\lambda_1^2\lambda_2 - \lambda_2^2\lambda_1)^2}, \quad (11)$$

式中: $e_{\lambda}$ 表示谷值波长的测量精度。取 SM125 的波长测量精度 1 pm,从图 3 中提取的典型光谱的特征谷值波长  $\lambda_1 = 1546.041$  nm,  $\lambda_2 = 1553.696$  nm,  $\lambda_3 = 1562.240$  nm,代入式(11)计算可得耦合相移的最大误差为  $\delta_{\max} = 2.378 \times 10^{-4}$  rad = 0.0136°。

### 3 实验结果及讨论

#### 3.1 2×2 耦合器耦合相移检测

基于图 2,搭建了 2×2 单模光纤耦合器耦合相移测量装置,利用隔离器将 SM125 的 CH4 设为单向测量通道,光源从 P1 输入,由通道 1 和通道 4 同步采集互易端口 P1、非互易端口 P2 的干涉光谱。混合 Sagnac 干涉仪中保偏光纤长度约为 50 cm,实测的互易和非互易端口的输出光谱如图 4 所示。选取耦合器工作波长 1550 nm 附近的一个周期,利用 SM125 自动寻峰算法提取特征谷值波长,根据式(10)计算耦合器相移。为了提高检测准确性,在相同测量条件下多次采集光谱,计算耦合相移,检测结果如表 1 所示,取五次检测的平均值作为最终的相移检测结果,得到该 2×2 耦合器的耦合相移为

89.515°,多次测量的标准差为 0.0028°。

采用上述测量装置对三种常用分光比(50:50、70:30、90:10)的 2×2 耦合器的耦合相移进行了检测,并测试了其实际分光比和附加损耗。根据式(3)估算了其耦合相移的理论范围,结果如表 2 所示,可以看出,耦合相移的实际测量结果均位于估算范围内,验证了检测技术的合理性。

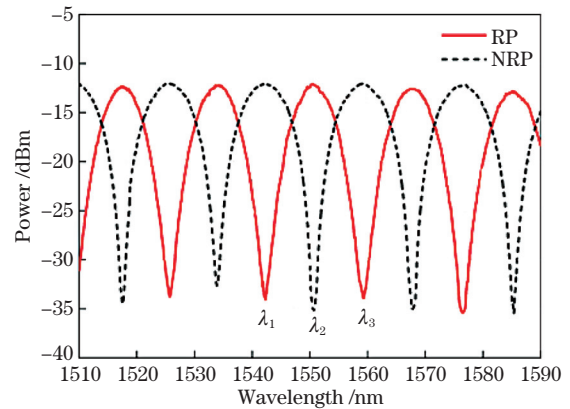


图 4 检测 2×2 单模耦合器的耦合相移时输出的光谱  
Fig. 4 Output spectra when detecting coupling phase shift of 2×2 single-mode coupler

表 1 2×2 耦合器的耦合相移重复测试结果

Table 1 Repeated test results of coupling phase shift of 2×2 coupler

No.	$\lambda_1$ /nm	$\lambda_2$ /nm	$\lambda_3$ /nm	$\Delta\varphi/(\circ)$	Average/ $(\circ)$	Standard deviation/ $(\circ)$
1	1542.092	1550.605	1559.306	89.516		
2	1542.166	1550.737	1559.499	89.511		
3	1542.163	1550.696	1559.418	89.515	89.515	0.0028
4	1542.086	1550.552	1559.204	89.519		
5	1542.122	1550.632	1559.330	89.516		

表 2 2×2 耦合器的耦合相移理论值与实测值的对比

Table 2 Comparison between theoretical and measured values of coupling phase shift of 2×2 coupler

Coupling ratio	$ s_{13} ^2$	$ s_{14} ^2$	Additional loss	Theoretical estimation range	Measured value
50:50	0.482	0.493	0.025	$86.985^\circ \leq \Delta\varphi \leq 93.015^\circ$	89.512°
70:30	0.297	0.670	0.033	$86.245^\circ \leq \Delta\varphi \leq 94.755^\circ$	90.602°
90:10	0.883	0.092	0.025	$81.141^\circ \leq \Delta\varphi \leq 98.859^\circ$	91.834°

由检测结果可知,由于附加损耗的存在,2×2 耦合器的实际耦合相移相对理想状态下的 90°有所偏移,随着分光比的增大,耦合相移的理论允许范围有所扩大,实测耦合相移值均处于理论估计范围内,

且有增大的趋势。

### 3.2 3×3 耦合器耦合相移检测

利用上述方法分别对 3×3 耦合器各端口间的耦合相移进行了检测,采用了与图2相同的光路连

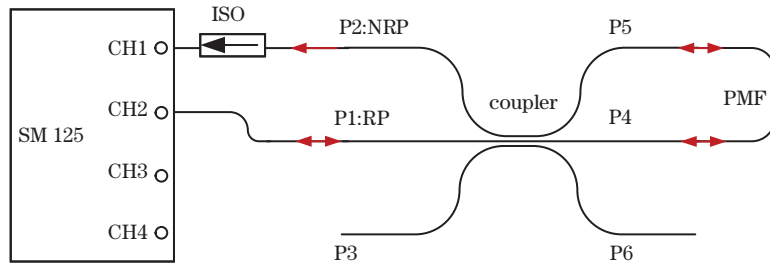


图 5 3×3 单模光纤耦合器耦合相移测量装置

Fig. 5 Device for coupling phase shift detection of 3×3 single-mode optical fiber coupler

接和测试过程。图 5 所示为端口 P4、P5 间耦合相移测试时的光路连接状态,其他端口间的耦合相移测试与此类似。实测互易和非互易端口的输出光谱如图 6 所示,测得端口 P4、P5 之间的耦合相移  $\Delta\varphi_{45} = 120.892^\circ$ 。改变检测端口和相应 Sagnac 环的连接端口,重复上述步骤,可测得 P6 和 P4 及 P5 和 P6 间的耦合相移。检测结果如表 3 所示,其中  $\Delta\varphi_{ij}$  表示耦合器端口  $i, j$  间的耦合相移,  $|s_c|^2$  为耦合臂的耦合效率,  $|s_d|^2$  为直通臂的耦合效率。可以看出,实际测量结果与理论估计范围相符,验证了该检测方案用于各类单模光纤耦合器相移检测的可行性和正确性。

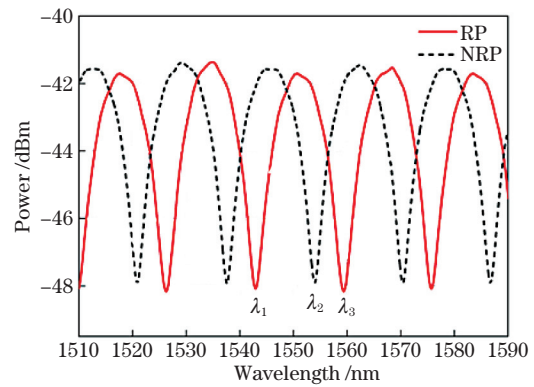


图 6 检测 3×3 单模耦合器的耦合相移时输出的光谱  
Fig. 6 Output spectra when detecting coupling phase shift of 3×3 single-mode coupler

表 3 3×3 耦合器耦合相移理论值与实测值的对比

Table 3 Comparison between theoretical and measured values of coupling phase shift of 3×3 coupler

$ s_d ^2$	$ s_c ^2$	Additional loss	Theoretical estimation range	$\Delta\varphi_{45}$		$\Delta\varphi_{64}$		$\Delta\varphi_{56}$	
				Measured value / (°)	Standard deviation / (°)	Measured value / (°)	Standard deviation / (°)	Measured value / (°)	Standard deviation / (°)
0.313	0.332	0.023	$118.359^\circ \leq \Delta\varphi \leq 129.866^\circ$	120.888	0.0036	118.265	0.0035	120.829	0.0033

### 3.3 2×2 耦合器耦合相移的温度敏感特性检测

在光纤传感系统中,系统的温度稳定性是一项重要指标。研究表明,温度变化会影响耦合器的耦合相移<sup>[24]</sup>,进而影响光纤干涉传感系统的温度稳定性。由理论分析可知,耦合相移与损耗和分光比有关,而根据熔锥型光纤耦合器的制作原理<sup>[25]</sup>,温度变化会引起耦合器耦合参数的改变,进而改变耦合器相移。

为了确定不同温度下由耦合器耦合相移变化造成的光纤传感系统的性能漂移,我们利用本文提出的检测技术,对 2×2 耦合器耦合相移的温度敏感特性进行了实验检测。实验中,将耦合器置于温箱内,

在不同温度下进行耦合相移检测,温度检测范围为 -40~60 °C,间隔为 20 °C,在每个温度点处维持 30 min,同一温度点采集 5 组光谱数据,计算耦合相移并取均值作为检测结果,对两只不同批次的 2×2 耦合器进行了耦合相移温度敏感特性检测,拟合后得到其温度-相移关系曲线,如图 7 所示。

实验结果表明,2×2 耦合器的耦合相移随温度的升高有减小的趋势,但不同批次耦合器的温度敏感性各不相同。采用本文提出的耦合器相移检测方法,首次实现了耦合相移温度稳定性的测试,为高稳定性耦合器的研制和筛选提供了有效手段。

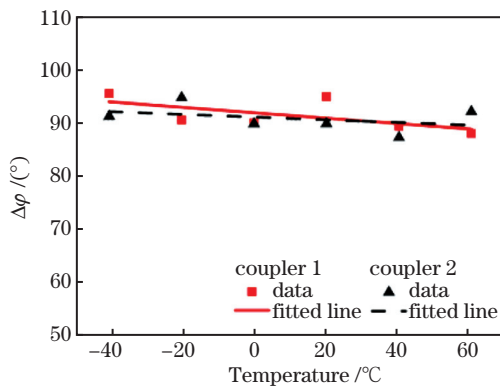


图 7  $2 \times 2$  耦合器的耦合相移温度敏感特性检测结果

Fig. 7 Test results of temperature sensitive characteristics of coupling phase shift of  $2 \times 2$  coupler

## 4 结 论

提出了一种基于混合 Sagnac 干涉仪的新型光纤耦合器耦合相移检测技术,基于互易端口和非互易端口输出光谱的谷值波长特征,实现了单模光纤耦合器耦合相移的检测,检测精度可达  $0.0136^\circ$ ,相对现有的耦合器相移检测方法,检测精度提高了一个数量级。搭建了实验系统,实现了固定分光比  $3 \times 3$  单模耦合器以及不同分光比的  $2 \times 2$  单模耦合器耦合相移的检测,检测结果与理论估计一致,多次检测的最大标准差为  $0.0036^\circ$ 。利用该检测技术还实现了不同温度条件下  $2 \times 2$  单模耦合器的相移变化测量。理论分析和实验研究表明,所提方案具有结构简单、抗干扰能力强、计算简便、检测精度高等特性,适用于各类多端口单模光纤耦合器的耦合相移检测,为光纤耦合器耦合相移的定量测试和分析提供了精确有效的手段,并为相位稳定耦合器的研制和筛选提供了重要参考。

## 参 考 文 献

- [1] 林锦海, 张伟刚. 光纤耦合器的理论、设计及进展[J]. 物理学进展, 2010, 30(1): 37-80.  
Lin J H, Zhang W G. Recent progress in theory, design and development of fiber coupler[J]. Progress in Physics, 2010, 30(1): 37-80.
- [2] 郝晋青, 韩丙辰. 基于游标效应的高灵敏度光纤耦合器折射率传感器[J]. 光学学报, 2020, 40(2): 0206002.  
Hao J Q, Han B C. Ultrasensitive refractive index sensor based on optical fiber couplers assisted with vernier effect[J]. Acta Optica Sinica, 2020, 40(2): 0206002.
- [3] 曾周末, 刘芳, 封皓, 等. 基于  $3 \times 3$  耦合器的双马赫-曾德尔干涉仪数字化相位解调[J]. 光学精密工

程, 2014, 22(6): 1410-1417.

Zeng Z M, Liu F, Feng H, et al. Digitalized demodulation based on  $3 \times 3$  coupler for dual Mach-Zehnder fiber interferometer[J]. Optics and Precision Engineering, 2014, 22(6): 1410-1417.

- [4] 何俊, 肖浩, 冯磊, 等. 基于  $3 \times 3$  耦合器的迈克耳孙干涉仪相位特性分析[J]. 光学学报, 2008, 28(10): 1867-1873.  
He J, Xiao H, Feng L, et al. Analysis of phase characteristics of fiber Michelson interferometer based on a  $3 \times 3$  coupler[J]. Acta Optica Sinica, 2008, 28(10): 1867-1873.
- [5] Sheem S K. Optical fiber interferometers with  $[3 \times 3]$  directional couplers: analysis[J]. Journal of Applied Physics, 1981, 52(6): 3865-3872.
- [6] Sheem S K. Fiber-optic gyroscope with  $[3 \times 3]$  directional coupler[J]. Applied Physics Letters, 1980, 37(10): 869-871.
- [7] 汪云云, 黄俊斌, 丁朋, 等. 实时修正零差对称算法解调 DFB 光纤激光水听器[J]. 中国激光, 2021, 48(13): 1306001.  
Wang Y Y, Huang J B, Ding P, et al. Real-time correction homodyne symmetry algorithm to demodulate DFB fiber laser hydrophone[J]. Chinese Journal of Lasers, 2021, 48(13): 1306001.
- [8] Bechtle J, Trommer G F. A new measurement algorithm for the  $3 \times 3$  fiber optic Sagnac interferometer[J]. Proceedings of SPIE, 2005, 5855: 944-947.
- [9] 梅泽, 吕海飞, 文晓艳, 等. 改进的椭圆拟合算法及振动传感相位解调[J]. 光学学报, 2021, 41(24): 2412001.  
Mei Z, Lü H F, Wen X Y, et al. The modified ellipse fitting algorithm and phase demodulation of vibration sensing[J]. Acta Optica Sinica, 2021, 41(24): 2412001.
- [10] Priest R G. Analysis of fiber interferometer utilizing  $3 \times 3$  fiber coupler[J]. IEEE Transactions on Microwave Theory and Techniques, 1982, 30(10): 1589-1591.
- [11] Pietzsch J. Scattering matrix analysis of  $3 \times 3$  fiber couplers[J]. Journal of Lightwave Technology, 1989, 7(2): 303-307.
- [12] 张清华.  $3 \times 3$  光纤耦合器散射矩阵参数的对称算子法分析[J]. 光纤与电缆及其应用技术, 1999, 1(1): 18-20.  
Zhang J H. Analysis of the scattering matrix parameters of  $3 \times 3$  optical fiber coupler by symmetry operator method[J]. Optical Fiber & Electric Cable, 1999, 1(1): 18-20.
- [13] Gottwald E, Pietzsch J. Measurement method for

- determination of optical phase shifts in  $3 \times 3$  fibre couplers[J]. *Electronics Letters*, 1988, 24(5): 265-266.
- [14] Schliep F, Hereth R. Phase sensitive measurement technique for singlemode fibre directional couplers [J]. *Electronics Letters*, 1992, 28(16): 1538-1540.
- [15] Schliep F, Hereth R, Schiffner G. Phase sensitive investigations of  $3 \times 3$  singlemode fibre directional couplers[J]. *Electronics Letters*, 1993, 29(1): 68-70.
- [16] 崔杰, 刘亭亭, 肖灵, 等. 一种确定光纤传感器中  $3 \times 3$  耦合器输出信号相位差的新算法 [J]. *应用声学*, 2008, 27(1): 36-41.  
Cui J, Liu T T, Xiao L, et al. A new algorithm to determine the phase difference of the outputs of a  $3 \times 3$  fiber-optic coupler [J]. *Applied Acoustics*, 2008, 27(1): 36-41.
- [17] Jiang Y, Liang P J, Jiang T F. Direct measurement of optical phase difference in a  $3 \times 3$  fiber coupler[J]. *Optical Fiber Technology*, 2010, 16(3): 135-139.
- [18] 张靖华. 损耗对光纤耦合器输出相位差的影响 [J]. *光纤与电缆及其应用技术*, 1999, 6(6): 17-21.  
Zhang J H. Effect of loss on output phase differences of optical fiber couplers[J]. *Optical Fiber & Electric Cable and Their Applications*, 1999, 6(6): 17-21.
- [19] 张桂才. 光纤陀螺原理与技术 [M]. 北京: 国防工业出版社, 2008: 37-42.  
Zhang G C. The principles and technologies of fiber-optic gyroscope [M]. Beijing: National Defense Industry Press, 2008: 37-42.
- [20] 李海岗. 基于光纤光栅传感器的铝电解槽高温安全监测系统 [D]. 济南: 山东大学, 2008: 27-30.  
Li H G. Aluminium electro-bath's high temperature safe monitor system based on fiber grating sensor [D]. Jinan: Shandong University, 2008: 27-30.
- [21] McBride R, Jones J D C. A passive phase recovery technique for Sagnac interferometers based on controlled loop birefringence [J]. *Journal of Modern Optics*, 1992, 39(6): 1309-1320.
- [22] Yang Y H, Duan W Q, Ye M. High precision measurement technology for beat length of birefringence optical fiber [J]. *Measurement Science and Technology*, 2013, 24(2): 025201.
- [23] 费业泰. 误差理论与数据处理 [M]. 7 版. 北京: 机械工业出版社, 2015: 62-64.  
Fei Y T. Error theory and data processing [M]. 7th ed. Beijing: China Machine Press, 2015: 62-64.
- [24] Davis M A, Kersey A D, Marrone M J, et al. Characterization of  $3 \times 3$  fiber couplers for passive homodyne systems: polarization and temperature sensitivity [C] // *Optical Fiber Communication Conference*, February 6, 1989, Houston, Texas. Washington, D.C.: OSA, 1989: WQ2.
- [25] 周梦薇, 朱益清, 姚晓天. 熔锥型微纳光纤耦合器的理论与实验研究 [J]. *光子学报*, 2020, 49(5): 0506005.  
Zhou M W, Zhu Y Q, Yao X T. Theoretical and experimental analysis of fused biconical microfiber coupler [J]. *Acta Photonica Sinica*, 2020, 49(5): 0506005.

## Coupling Phase Shift Detection Technology of Fiber Coupler Based on Sagnac Interferometer

Wang Ruiqin, Yang Yuanhong\*, Li Hui

*School of Instrumentation Science and Opto-Electronics Engineering, Beihang University, Beijing 100191, China*

### Abstract

**Objective** The optical fiber coupler is the basic device in an optical fiber sensor system. The phase relationship between the outputs of the coupler, that is, the coupling phase shift, has a significant impact on the performance of the sensor system. An accurate measurement of the coupling phase shift and its variation characteristics are of great value to the development of high-performance fiber couplers and the improvement in the performance of their application systems. As the mainstream method for the theoretical analysis of coupling phase shifts, the scattering matrix analysis method has many ideal assumptions in the analysis process, resulting in a large gap between the calculated results and real phase shifts. Besides, the coupling phase shift is susceptible to external factors such as temperature. Therefore, the theoretical analysis has great limitations, and the exact coupling phase shift value must be determined through the experimental test. At present, the existing experimental detection scheme is based on the Mach-Zehnder interferometer, and the coupling phase shift is calculated by detecting the output power of each port using the phase modulation technology. The detection accuracy is influenced by photoelectric conversion, optical path

loss, coupler performance, modulation signal, and other factors, and thus there is a large error. The highest detection accuracy that can be achieved in the existing reports is  $0.229^\circ$ . In this study, we propose a novel coupling phase shift detection technology based on the hybrid Sagnac interferometer, which uses wavelength demodulation to achieve the coupling phase shift detection, so as to improve the detection accuracy and the anti-interference of the detection device. It is hoped that the proposed detection technology can provide an effective means for the quantitative and accurate test and analysis of the coupling phase shift of the single-mode fiber coupler.

**Methods** The coupling phase shift detection technology proposed in this paper is based on a hybrid Sagnac interferometer structure, which is composed of the single-mode fiber coupler to be tested and a polarization maintaining fiber. The fiber spectral demodulator is used to provide the scanning light source and simultaneously detect the output interference spectra of its reciprocal port and non-reciprocal port. Due to the reciprocity of the Sagnac optical path, the relative phase shift of the output spectra at both ports is twice the coupling phase shift. Therefore, the valley wavelength characteristics of the two interference spectra are extracted for calculation to obtain the coupling phase shift value of the fiber coupler, and thus the measurement of the coupling phase shift is realized. According to the proposed detection scheme, the experimental system is built to realize the coupling phase shift detection of  $2 \times 2$  single-mode couplers with different splitting ratios and  $3 \times 3$  single-mode couplers. Moreover, the coupling phase shift characteristics of the  $2 \times 2$  single-mode couplers at different temperature conditions are studied for the first time.

**Results and Discussions** In this paper, the limit error of the proposed detection scheme is analyzed theoretically, and the detection accuracy is  $0.0136^\circ$ . The effectiveness and stability of the scheme are verified by experiments. First, the coupling phase shifts of  $2 \times 2$  single-mode fiber couplers with three common splitting ratios (10:90, 30:70, 50:50) are detected, the experimental results are consistent with the theoretical results (Table 2), and the standard deviation of multiple measurements is  $0.0028^\circ$  (Table 1). Due to the existence of additional loss, the actual coupling phase shift of the  $2 \times 2$  coupler is deviated from the ideal  $90^\circ$ , and with the increase of splitting ratio, the coupling phase shift has a gradual upward trend. Second, the coupling phase shift among the three ports of the  $3 \times 3$  coupler is detected by the detection scheme. The measurement results are also consistent with the theoretical estimation range, and the maximum standard deviation is  $0.0036^\circ$  (Table 3), which verifies the feasibility and correctness of the detection scheme applied to the coupling phase shift detection of various single-mode fiber couplers. Finally, the temperature experiment result (Fig. 7) shows that the coupling phase shift of the  $2 \times 2$  coupler decreases with the increase of temperature, but the temperature sensitivities of different batches of couplers are different. The coupling phase shift detection method proposed in this paper can be used to test the temperature stability and other related characteristics of the coupling phase shift, which provides an effective means for the development of high-stability couplers and the selection of couplers.

**Conclusions** In present study, a novel coupling phase shift detection technology of a single-mode fiber coupler based on the hybrid Sagnac interferometer is proposed. According to the valley wavelength characteristics of its reciprocal port and non-reciprocal port output spectra, the detection of the coupling phase shift of the single-mode fiber coupler is realized, and the detection accuracy can reach  $0.0136^\circ$ , which is an order of magnitude higher than the existing coupling phase shift detection accuracy ( $0.229^\circ$ ). The experimental system is built to realize the detection of the coupling phase shifts of  $3 \times 3$  single-mode coupler with the fixed splitting ratio and  $2 \times 2$  single-mode couplers with different splitting ratios. The detection results are consistent with theoretical estimates, and the maximum standard deviation of multiple detection is  $0.0036^\circ$ . The proposed detection method is also used to measure the coupling phase shift change of the  $2 \times 2$  single-mode coupler at different temperatures for the first time. The research shows that the proposed detection method has advantages in simplicity, detection accuracy, and adaptability. It can be used for the quantitative and accurate measurement and analysis of coupling phase shift of various multi-port single-mode fiber couplers, and provides an important technical support for the development and screening of phase stabilizer couplers.

**Key words** fiber optics; single-mode fiber coupler; coupling phase shift; Sagnac interferometer